Research Square

Preprints are preliminary reports that have not undergone peer review.
They should not be considered conclusive, used to inform clinical practice,
or referenced by the media as validated information.

Neratinib enhances trastuzumab emtansine trafficking and antitumor activity in breast cancer models

Meng-Ching Yeh
Hsinchu MacKay Memorial Hospital
Shih-Ping Cheng
MacKay Memorial Hospital
Ming-Jen Chen
MacKay Memorial Hospital
Shao-Chiang Chang
Mackay Memorial Hospital
Yuan-Ching Chang
changyc@mmh.org.tw

MacKay Memorial Hospital

Article

Keywords: HER2, trastuzumab emtansine, neratinib, tucatinib, breast cancer

Posted Date: November 19th, 2026

DOI: https://doi.org/10.21203/rs.3.rs-11496490/v1

License: This work is licensed under a Creative Commons Attribution 4.0 International License.
Read Full License

Additional Declarations: No competing interests reported.

Abstract

Purpose

The efficacy of trastuzumab emtansine (T-DM1) relies on HER2 binding, internalization, intracellular processing, and payload delivery. We investigated how neratinib and tucatinib differentially affect T-DM1 trafficking and antitumor activity in breast cancer models.

Methods

HER2-expressing breast cancer cells were treated with T-DM1 alone or in combination with neratinib or tucatinib, and cell viability was assessed by CCK-8 assay. pHrodo-labeled T-DM1 was used to quantify acidification-associated intracellular accumulation. HER2 phosphorylation and HER2-associated ubiquitination were examined by immunoblotting and immunoprecipitation. Antitumor activity was evaluated in HCC1954 orthotopic xenografts.

Results

Neratinib enhanced T-DM1-mediated viability reduction from 51.7% to 31.0% in SK-BR-3 cells and from 37.4% to 19.3% in HCC1954 cells. In contrast, tucatinib did not significantly augment T-DM1 activity. Neratinib increased the pHrodo-T-DM1 fluorescence index and HER2-associated ubiquitin signal, while both kinase inhibitors reduced HER2 phosphorylation. Dynasore, an inhibitor of dynamin-dependent endocytosis, reduced pHrodo fluorescence and partially reversed the observed viability loss. In cells with lower ERBB2 transcript expression, the combination effects were modest. In xenografts, T-DM1 combined with neratinib significantly reduced tumor growth compared to T-DM1 alone and was associated with reduced HER2-pathway phosphorylation and increased caspase-3 cleavage.

Conclusion

We demonstrate that neratinib may potentiate T-DM1 activity, which is associated with increased accumulation in acidic compartments and increased HER2-associated ubiquitination. These findings support further evaluation of neratinib as a combination partner with T-DM1, particularly regarding productive payload delivery and treatment scheduling.

Introduction

Trastuzumab emtansine (T-DM1) combines HER2 recognition with the delivery of the microtubule inhibitor DM1 and is effective in metastatic and residual invasive HER2-positive breast cancer [1, 2]. Its activity depends on steps beyond receptor binding, including internalization, intracellular processing, and payload action. Variability in these processes can reduce efficacy despite HER2 expression [3].

Therefore, defining how concurrent HER2-targeted drugs affect antibody–drug conjugate (ADC) trafficking may guide combination strategies.

HER2 tyrosine kinase inhibitors (TKIs) differ in target selectivity, binding reversibility, and effects on receptor handling. In breast cancer cells, neratinib has been reported to promote HER2 ubiquitination and degradation by dissociating HER2 from HSP90 [4]. In ERBB2-amplified or mutant lung cancer models, neratinib increased HER2-mediated internalization of cytotoxic agents [5]. By contrast, Olson et al. showed that tucatinib increased surface HER2 availability and enhanced T-DM1 activity in several breast cancer models, despite initially slowing antibody internalization [6]. These findings indicate that early internalization and sustained productive ADC delivery may not change in parallel.

In this study, we compared T-DM1 combined with neratinib or tucatinib in breast cancer models. We assessed viability, pH-sensitive ADC trafficking, HER2-associated ubiquitination, and orthotopic tumor growth. Our aim was to determine whether neratinib or tucatinib differentially affects T-DM1 activity and intracellular trafficking in HER2-positive breast cancer models, and to explore whether altered HER2 processing is associated with treatment response.

Materials and methods

Cell culture and reagents

SK-BR-3, HCC1954, BT-20, and MDA-MB-468 cells were obtained from the American Type Culture Collection (Manassas, VA, USA). Cells were maintained at 37°C in McCoy's 5a, RPMI-1640, Eagle's minimum essential medium, and Leibovitz's L-15 medium, respectively, each supplemented with 10% fetal bovine serum (FBS). T-DM1 was obtained from Roche (Basel, Switzerland). Neratinib, tucatinib, and dynasore were obtained from TargetMol Chemicals (Boston, MA, USA) and prepared as 10 mM stock solutions in dimethyl sulfoxide (DMSO).

Cell viability

Cells were plated at optimized densities in 96-well plates. After 24 h, the culture medium was replaced with fresh medium containing the indicated drug concentration or an equivalent volume of DMSO as a vehicle control. Viability was measured after 48 h using Cell Counting Kit-8 (Sigma-Aldrich, St. Louis, MO, USA), with absorbance normalized to vehicle-treated controls. For the HER2-positive cell experiments, T-DM1, neratinib, and tucatinib were used at concentrations of 0.04 μg/mL, 25 nM, and 300 nM, respectively. Dynasore was used at 50 μM in SK-BR-3 cells and 15 μM in HCC1954 cells. Single agents and combinations were compared at the indicated concentrations.

Fluorescence trafficking assay

T-DM1 was labeled using the pHrodo iFL Red Microscale Protein Labeling Kit (Thermo Fisher Scientific, Waltham, MA, USA). A labeling solution (10 µL, 2 mM) was incubated with T-DM1 (5 µL, 20 mg/mL) for 30 min at room temperature, followed by resin-column purification at 1,000 × g for 5 min. SK-BR-3 cells (approximately 3×10^4/well) were plated for 24 h, then incubated for 1 h at 4°C in medium containing 2% FBS, pHrodo-T-DM1 (0.05 µg/mL), and Hoechst 33342 (20 µM). Plates were then transferred to 37°C. Neratinib (25 nM) or tucatinib (300 nM) was added with labeled T-DM1; dynasore (50 µM) was used as a 30-min pretreatment where indicated.

Images were acquired at 0, 5, 24, 48, and 72 h using an Olympus IX71 inverted fluorescence microscope (Olympus, Tokyo, Japan) and analyzed with ImageJ version 1.54 (National Institutes of Health, Bethesda, MD, USA). The trafficking index was calculated as total cytoplasmic red fluorescence divided by the corresponding cell count. Because pHrodo fluorescence increases in acidic environments, this assay measures acidification-associated intracellular accumulation rather than directly measuring internalization rate or payload release.

Immunoblotting and HER2 immunoprecipitation

SK-BR-3 cells were treated for 5 h with T-DM1 (0.05 µg/mL), neratinib (25 nM), or tucatinib (300 nM), alone or in combination. Whole-cell proteins were separated by polyacrylamide gel electrophoresis and transferred to nitrocellulose membranes, as previously described [7]. After blocking with 5% skim milk, membranes were incubated overnight with antibodies against phospho-HER2 Tyr1248 (1:1000; #2247; Cell Signaling Technology, Danvers, MA, USA), total HER2 (1:1000; #2248; Cell Signaling Technology), ubiquitin (1:1000; #05-944; Sigma-Aldrich), and GAPDH (1:10,000; GTX627408; GeneTex, Irvine, CA, USA).

For HER2 immunoprecipitation, the Dynabeads Co-Immunoprecipitation Kit (Thermo Fisher Scientific) was used with anti-HER2 (GeneTex, GTX22428; approximately 5 µg antibody/mg beads). Cells were treated identically in the presence of 10 µM MG-132 (Selleck Chemicals, Houston, TX, USA) to inhibit proteasomal degradation. Lysates were incubated with 1.5 mg of antibody-coupled beads for 20 min at 4°C with rotation. The beads were then washed, and bound proteins were eluted by boiling in sample buffer. Normal IgG served as the negative immunoprecipitation control.

Quantitative reverse transcription PCR

RNA was isolated using TRIzol Reagent (Thermo Fisher Scientific) and quantified with a NanoDrop 2000 spectrophotometer (Thermo Fisher Scientific). Following reverse transcription, quantitative PCR was performed using SYBR Green Master Mix and an Applied Biosystems 7500 Fast Real-Time PCR System (Thermo Fisher Scientific). No-template negative controls were included in each assay. Relative expression levels were calculated by the comparative threshold-cycle method, using GAPDH as the reference and BHT-101 cells as the calibrator. ERBB2 primer sequences were forward 5'-

CCCAGAATGGCTCAGTGACC-3' and reverse 5'-GGCATGTAGGAGAGGTCAGG-3'; GAPDH primer sequences were forward 5'-CTCCTCCACCTTTGACGCTG-3' and reverse 5'-CTCCTTGGAGGCCATGTGG-3'.

Orthotopic xenografts

All animal procedures were approved by the Institutional Animal Care and Use Committee of MacKay Memorial Hospital (approval no. MMH-A-S-114-08) and were performed in accordance with the relevant institutional guidelines and regulations regarding the care and use of laboratory animals. Twenty-four six-week-old female BALB/c nude mice were obtained from the National Center for Biomodels, Taipei, Taiwan. HCC1954 cells (approximately 2.5×10^6 in 50 μL of 1:1 phosphate-buffered saline/Matrigel) were injected into the bilateral fourth mammary fat pads. Tumor dimensions were measured every 3 days, and tumor volume was calculated as length × width^2/2.

Mice were randomized into six groups (four mice/group): vehicle control, T-DM1, neratinib, tucatinib, T-DM1 plus neratinib, or T-DM1 plus tucatinib. T-DM1 was administered intravenously at 0.5 mg/kg every 3 weeks. Neratinib and tucatinib were administered orally at 10 mg/kg five times per week. Tumor measurements and data analysis were performed blinded to group allocation.

Tumor xenograft implantation and drug administration via oral gavage and tail vein injection were performed without analgesic medication. Animals were monitored regularly for signs of pain, distress, or adverse effects throughout the study. The primary study endpoint was tumor volume. Humane endpoints were established to minimize animal suffering and included excessive tumor burden, defined as tumor weight exceeding 10% of body weight, or signs of poor health or clinical deterioration. Animals reaching humane endpoints were removed from the study and euthanized by carbon dioxide inhalation in accordance with institutional animal care and use guidelines. Euthanasia was performed using an approved protocol to minimize pain and distress, and death was confirmed before tissue collection or disposal.

Excised tumors were subjected to immunoblot analysis using the following primary antibodies: phospho-HER2 Tyr1248 (#2247; Cell Signaling Technology), phospho-AKT Ser473 (#9271; Cell Signaling Technology), phospho-ERK1/2 Thr202/Tyr204 (#9101; Cell Signaling Technology), γ-H2AX Ser139 (ab18311; Abcam, Cambridge, UK), and caspase-3 (GTX110543; GeneTex).

Statistical analysis

In vitro experiments were performed independently at least three times. For xenograft analyses, individual mice served as the experimental unit (n = 4 per treatment group). The volumes of the two tumors in each mouse were averaged at each time point before group-level analysis. Data are expressed as mean ± standard deviation. Analyses used one-way analysis of variance (ANOVA) or two-way repeated-measures ANOVA with Tukey's multiple-comparison test in GraphPad Prism 8.3.0. All tests were two-sided, with $P < 0.05$ considered significant.

Results

Neratinib enhanced viability reduction by T-DM1

The combination of T-DM1 and neratinib significantly reduced viability from 51.7 ± 4.8% to 31.0 ± 4.0% in SK-BR-3 cells and from 37.4 ± 6.6% to 19.3 ± 4.4% in HCC1954 cells compared to T-DM1 alone ($P = 0.0002$ and $P = 0.040$, respectively; Fig. 1). In contrast, the combination of tucatinib and T-DM1 resulted in relative cell viabilities of 51.3% ± 7.8% in SK-BR-3 cells and 52.0% ± 13.2% in HCC1954 cells and did not significantly reduce viability compared to T-DM1 alone.

In SK-BR-3 cells, dynasore, an inhibitor of dynamin-dependent endocytosis, increased viability to 74.0 ± 7.2% during T-DM1 treatment ($P < 0.0001$) and to 46.6 ± 3.1% during T-DM1 plus neratinib treatment ($P = 0.010$). Its effect during T-DM1 plus tucatinib treatment was not significant (64.4 ± 6.2%; $P = 0.069$). Notably, dynasore alone did not significantly affect SK-BR-3 viability compared to vehicle control ($P = 0.068$), but it did reduce HCC1954 viability to 72.6 ± 10.0% ($P = 0.0009$) at a dose as low as 15 μM. In HCC1954 cells, dynasore did not significantly reverse the effect of T-DM1 plus neratinib, with viability at 31.0 ± 5.9% ($P = 0.555$).

Neratinib increased acidic compartment accumulation and HER2-associated ubiquitination

We evaluated the internalization of T-DM1 labeled with pHrodo, a pH-sensitive dye that fluoresces only at low pH, providing fluorescent evidence of ligand-receptor endocytosis. Neratinib enhanced pHrodo-T-DM1 fluorescence from early time points throughout the entire observation period (Fig. 2). At 72 h, the trafficking index was higher with neratinib than with T-DM1 alone ($P = 0.049$) or T-DM1 plus tucatinib ($P = 0.033$). Dynasore reduced this neratinib-associated increase ($P = 0.008$), though some residual fluorescence persisted.

At 5 h, T-DM1 increased HER2 Tyr1248 phosphorylation, indicating active HER2 receptor signaling, while both TKIs reduced it. Total HER2 levels appeared similar across all treatments (Fig. 3). Neratinib-containing treatments showed a stronger ubiquitin signal in HER2 immunoprecipitates, whereas tucatinib did not exhibit a comparable increase. These findings suggest a link between enhanced HER2-associated ubiquitination and ubiquitin-mediated internalization and lysosomal trafficking.

Effects were modest in cells with lower ERBB2 transcript expression

We examined the ERBB2 transcript levels of a panel of cell lines in our laboratory (Fig. 4A). Compared with BHT-101, expression was 837.7-fold higher in HCC1954 cells and 113.0-fold higher in SK-BR-3 cells, but only 20.2-fold higher in BT-20 cells and 6.9-fold higher in MDA-MB-468 cells. BT-20 was chosen as a HER2-low cell line and MDA-MB-468 as a HER2-ultralow cell line.

In BT-20 cells, T-DM1 plus neratinib reduced viability to 91.8 ± 3.0%. This was significantly lower than the vehicle control (P = 0.002), T-DM1 alone (P = 0.014), and neratinib alone (P = 0.001; Fig. 4B). In MDA-MB-468 cells, the combination of neratinib and T-DM1 reduced viability to 90.0 ± 3.5%. This was lower than the vehicle control (P = 0.001) and neratinib alone (P = 0.0003), but not significantly different from T-DM1 alone (P = 0.104). Combined tucatinib and T-DM1 treatment did not significantly enhance viability reduction beyond that of the corresponding single agents.

Neratinib enhanced T-DM1 activity in orthotopic tumors

T-DM1 reduced HCC1954 xenograft growth compared with vehicle control (P = 0.031), whereas neither TKI alone significantly affected growth (Fig. 5A). The combination of T-DM1 and neratinib further reduced growth compared with vehicle control (P = 0.0002), T-DM1 alone (P = 0.008), and neratinib alone (P = 0.003). In contrast, T-DM1 plus tucatinib did not differ significantly from vehicle control or either single agent.

Tumor blots showed lower phospho-HER2, phospho-AKT, and phospho-ERK1/2 expression levels with T-DM1 plus neratinib (Fig. 5B). Both combinations showed prominent γ-H2AX signals, and caspase-3 cleavage was more evident with the neratinib combination. These results are in agreement with the augmented antitumor activity of T-DM1 combined with neratinib observed in vitro.

Discussion

This study links enhanced T-DM1 activity with increased accumulation in acidic intracellular compartments under defined treatment conditions. Neratinib augmented viability reduction in HER2-positive cell lines, increased pHrodo-T-DM1 signal and HER2-associated ubiquitination, and potentiated tumor growth inhibition in HCC1954 xenografts. In contrast, tucatinib reduced HER2 phosphorylation but did not significantly increase viability reduction over T-DM1 alone. These observations support assessing ADC handling alongside kinase inhibition.

The neratinib-associated phenotype is consistent with reports of HSP90 dissociation, HER2 ubiquitination, and endocytic degradation in breast cancer [4], and enhanced ADC internalization in ERBB2-altered lung cancer [5]. A conference abstract described favorable T-DM1 interactions with irreversible TKIs in breast cancer cells [8], while a subsequent study reported enhanced T-DM1 endocytosis with pyrotinib [9]. Together, these studies provide a rationale for testing whether receptor processing contributes to combination activity. Nevertheless, broader drug-response variation argues against using inhibitor reversibility alone to select an ADC partner [10].

The comparison with Olson et al. suggests that early uptake and sustained productive delivery are distinct endpoints [6]. In their breast cancer models, tucatinib initially slowed antibody internalization while increasing surface HER2, followed by lysosomal delivery and intracellular Lys-MCC-DM1 accumulation during sustained exposure. Retention could therefore preserve receptors for subsequent ADC binding and delivery. Their 96-h viability dose matrices also differed from our 48-h fixed-dose assay.

Our pHrodo-T-DM1 endpoint did not measure internalization rate or active catabolite production; therefore, higher fluorescence does not establish greater cumulative payload delivery. The two studies may capture different stages of ADC processing rather than mutually exclusive mechanisms.

Other studies reinforce the importance of receptor availability and downstream processing. Lapatinib-induced HER2 stabilization can enhance trastuzumab-dependent cytotoxicity [11], while signaling inhibition, PMCA2, and caveolin-1 can influence receptor distribution and antibody access [12–15]. Changes in proliferation may also affect sensitivity to a microtubule-directed payload [16]. Conversely, preserved internalization does not ensure T-DM1 activity when lysosomal proteolysis is impaired [17]. SLC46A3-dependent catabolite transport [18, 19] and intracellular routing [20] further distinguish ADC uptake from productive payload delivery. These mechanisms provide context but were not directly tested in the present study. It should be noted that dynasore also has dynamin-independent effects [21], limiting its ability to establish the specific uptake pathway responsible for the observed benefit.

Clinical findings support further study but do not establish a preferred TKI partner. NSABP FB-10 demonstrated the feasibility and preliminary activity of neratinib plus T-DM1 [22]. However, its phase II expansion was inconclusive under prespecified decision rules despite responses in 7 of 22 patients [23]. Nonrandomized TBCRC 022 cohorts showed intracranial activity, including after prior T-DM1, although accrual ended early [24]. Subsequent patient-reported outcomes highlighted the gastrointestinal symptom burden [25]. These observations justify investigation but do not demonstrate trafficking-mediated resistance reversal. For tucatinib, phase Ib evidence [26] was followed by improved progression-free survival in the randomized HER2CLIMB-02 trial [27]. This clinical benefit emphasizes the need to interpret our results within the experimental exposure conditions.

In addition, T-DXd studies offer related, ADC-specific evidence. In gastric cancer models, pyrotinib increased HER2-associated ubiquitination, T-DXd uptake, and combination activity, whereas lapatinib did not augment the tested viability endpoint [28]. Activating ERBB2 mutations were associated with faster T-DXd internalization in breast cancer models and longer progression-free survival in a retrospective cohort, without establishing a TKI-mediated effect [29]. HER2CLIMB-04 showed activity with tucatinib plus T-DXd but no clear additional benefit relative to historical monotherapy results [30]. However, differences in linker, payload, genotype, and exposure prevent direct extrapolation to our T-DM1 findings.

Clinical delivery and pharmacokinetic evidence place the timing hypothesis in context. ZEPHIR linked low antibody uptake to poor T-DM1 response, and an exploratory analysis of the same trial implicated microenvironmental barriers [31, 32]. These findings concern tumor access rather than intracellular payload release. At 3.6 mg/kg every 3 weeks, mean peak serum conjugated T-DM1 concentrations were approximately 75–81 μg/mL, with a terminal half-life of approximately 3–4 days [33, 34]. Earlier productive delivery could be advantageous as exposure declines, but a serum half-life does not define the intracellular processing window. The delayed delivery reported with tucatinib [6] and associations between higher trough or cumulative exposure and favorable outcomes [35, 36] also support sustained ADC availability. These exposure–response associations are subject to confounding. Human serum

concentrations cannot be equated with tumor-accessible ADC or our culture concentrations of 0.04–0.05 μg/mL.

Several limitations in this study should be acknowledged. The pHrodo assay measures acidification-associated ADC accumulation rather than active payload release, and HER2-associated ubiquitin signals do not establish a causal trafficking mechanism. Dynasore toxicity further limits mechanistic inference. The fixed-dose design and small xenograft cohort also preclude conclusions regarding pharmacological synergy or comparative superiority. Nevertheless, the observed enhancement of T-DM1 activity supports further investigation of neratinib as a combination partner. Future studies linking intracellular catabolite formation to treatment response under exposure-matched schedules would help determine the contribution of productive ADC delivery.

Conclusion

Neratinib enhanced T-DM1 activity under the tested conditions, accompanied by increased accumulation in acidic compartments and HER2-associated ubiquitination. These findings support further evaluation of neratinib as a combination partner and identify productive intracellular delivery as a testable explanation for the benefit. Exposure-matched studies linking trafficking to active catabolite formation and antitumor response are needed to guide partner selection and treatment scheduling.

Declarations

Use of generative artificial intelligence

OpenAI ChatGPT assisted with manuscript editing. No experimental data or figures were generated using this tool.

Ethics approval

Animal experiments were approved by the Institutional Animal Care and Use Committee of MacKay Memorial Hospital (approval no. MMH-A-S-114-08).

Consent to participate

Not applicable.

Competing interests

The authors declare no competing interests.

Funding

This work was supported by MacKay Memorial Hospital research grants MMH-E-113-08, MMH-E-114-08, and MMH-E-115-08.

Author Contribution

MCY and YCC conceived and designed the study, performed the investigation and formal analysis, and drafted the manuscript.SPC performed the formal analysis and critically revised the manuscript.MJC contributed to study conception and investigation and critically revised the manuscript.SCC conducted the investigation and formal analysis.

Acknowledgements

None.

Data Availability

The data generated and analyzed during this study are available from the corresponding author upon reasonable request

References

1. Verma, S. et al. Trastuzumab emtansine for HER2-positive advanced breast cancer. *N Engl. J. Med.* **367** (19), 1783–1791. 10.1056/NEJMoa1209124 (2012).
2. von Minckwitz, G. et al. Trastuzumab Emtansine for Residual Invasive HER2-Positive Breast Cancer. *N Engl. J. Med.* **380** (7), 617–628. 10.1056/NEJMoa1814017 (2019).
3. Hunter, F. W. et al. Mechanisms of resistance to trastuzumab emtansine (T-DM1) in HER2-positive breast cancer. *Br. J. Cancer*. **122** (5), 603–612. 10.1038/s41416-019-0635-y (2020).
4. Zhang, Y. et al. Neratinib induces ErbB2 ubiquitylation and endocytic degradation via HSP90 dissociation in breast cancer cells. *Cancer Lett.* **382** (2), 176–185. 10.1016/j.canlet.2016.08.026 (2016).
5. Li, B. T. et al. HER2-Mediated Internalization of Cytotoxic Agents in ERBB2 Amplified or Mutant Lung Cancers. *Cancer Discov*. **10** (5), 674–687. 10.1158/2159-8290.CD-20-0215 (2020).
6. Olson, D. et al. HER2-Selective and Reversible Tyrosine Kinase Inhibitor Tucatinib Potentiates the Activity of T-DM1 in Preclinical Models of HER2-positive Breast Cancer. *Cancer Res. Commun.* **3** (9), 1927–1939. 10.1158/2767-9764.CRC-23-0302 (2023).
7. Lee, F. et al. Zinc finger protein 639 expression is a novel prognostic determinant in breast cancer. *J. Breast Cancer*. **28** (2), 86–98. 10.4048/jbc.2024.0224 (2025).

8. Ashfield, N., Mahdi, A. F., Conlon, N. T., Crown, J. & Collins, D. M. Reversible versus irreversible tyrosine kinase inhibitors (TKIs) combined with antibody-drug conjugates (ADCs) in HER2-positive (HER2+) breast cancer (BC) cell lines. *Cancer Res.* **83** (5 Suppl), P1–11. 10.1158/1538-7445.SABCS22-P1-11-10 (2023).
9. Ren, W. et al. Pyrotinib promotes the antitumor effect of T-DM1 by increasing drug endocytosis in HER2-positive breast cancer. *Sci. Rep.* **15** (1), 18625. 10.1038/s41598-025-03678-1 (2025).
10. Conlon, N. T. et al. Comparative analysis of drug response and gene profiling of HER2-targeted tyrosine kinase inhibitors. *Br. J. Cancer*. **124** (7), 1249–1259. 10.1038/s41416-020-01257-x (2021).
11. Scaltriti, M. et al. Lapatinib, a HER2 tyrosine kinase inhibitor, induces stabilization and accumulation of HER2 and potentiates trastuzumab-dependent cell cytotoxicity. *Oncogene* **28** (6), 803–814. 10.1038/onc.2008.432 (2009).
12. Jeong, J., Kim, W., Kim, L. K., VanHouten, J. & Wysolmerski, J. J. HER2 signaling regulates HER2 localization and membrane retention. *PLoS One*. **12** (4), e0174849. 10.1371/journal.pone.0174849 (2017).
13. Jeong, J. et al. PMCA2 regulates HER2 protein kinase localization and signaling and promotes HER2-mediated breast cancer. *Proc. Natl. Acad. Sci. U S A*. **113** (3), E282–E290. 10.1073/pnas.1516138113 (2016).
14. Pereira, P. M. R. et al. Caveolin-1 mediates cellular distribution of HER2 and affects trastuzumab binding and therapeutic efficacy. *Nat. Commun.* **9** (1), 5137. 10.1038/s41467-018-07608-w (2018).
15. Pereira, P. M. R. et al. Caveolin-1 temporal modulation enhances antibody drug efficacy in heterogeneous gastric cancer. *Nat. Commun.* **13** (1), 2526. 10.1038/s41467-022-30142-9 (2022).
16. Brasó-Maristany, F. et al. Phenotypic changes of HER2-positive breast cancer during and after dual HER2 blockade. *Nat. Commun.* **11** (1), 385. 10.1038/s41467-019-14111-3 (2020).
17. Ríos-Luci, C. et al. Resistance to the Antibody-Drug Conjugate T-DM1 Is Based in a Reduction in Lysosomal Proteolytic Activity. *Cancer Res.* **77** (17), 4639–4651. 10.1158/0008-5472.CAN-16-3127 (2017).
18. Tomabechi, R. et al. SLC46A3 is a lysosomal proton-coupled steroid conjugate and bile acid transporter involved in transport of active catabolites of T-DM1. *PNAS Nexus*. **1** (3), pgac063. 10.1093/pnasnexus/pgac063 (2022).
19. Li, G. et al. Mechanisms of Acquired Resistance to Trastuzumab Emtansine in Breast Cancer Cells. *Mol. Cancer Ther.* **17** (7), 1441–1453. 10.1158/1535-7163.MCT-17-0296 (2018).
20. Sung, M. et al. Caveolae-Mediated Endocytosis as a Novel Mechanism of Resistance to Trastuzumab Emtansine (T-DM1). *Mol. Cancer Ther.* **17** (1), 243–253. 10.1158/1535-7163.MCT-17-0403 (2018).
21. Park, R. J. et al. Dynamin triple knockout cells reveal off target effects of commonly used dynamin inhibitors. *J. Cell. Sci.* **126** (Pt 22), 5305–5312. 10.1242/jcs.138578 (2013).
22. Abraham, J. et al. Safety and Efficacy of T-DM1 Plus Neratinib in Patients With Metastatic HER2-Positive Breast Cancer: NSABP Foundation Trial FB-10. *J. Clin. Oncol.* **37** (29), 2601–2609.

10.1200/JCO.19.00858 (2019).

23. Jacobs, S. A. et al. NSABP FB-10: a phase Ib/II trial evaluating ado-trastuzumab emtansine (T-DM1) with neratinib in women with metastatic HER2-positive breast cancer. *Breast Cancer Res.* **26** (1), 69. 10.1186/s13058-024-01823-8 (2024).
24. Freedman, R. A. et al. Neratinib and ado-trastuzumab emtansine for pretreated and untreated human epidermal growth factor receptor 2 (HER2)-positive breast cancer brain metastases: Translational Breast Cancer Research Consortium trial 022. *Ann. Oncol.* **35** (11), 993–1002. 10.1016/j.annonc.2024.07.245 (2024).
25. Grinda, T. et al. Patient-reported outcomes from the TBCRC 022 study of neratinib and ado-trastuzumab emtansine for HER2-positive breast cancer brain metastases. *Breast* **89**, 104881. 10.1016/j.breast.2026.104881 (2026).
26. Borges, V. F. et al. Tucatinib Combined With Ado-Trastuzumab Emtansine in Advanced ERBB2/HER2-Positive Metastatic Breast Cancer: A Phase 1b Clinical Trial. *JAMA Oncol.* **4** (9), 1214–1220. 10.1001/jamaoncol.2018.1812 (2018).
27. Hurvitz, S. A. et al. Tucatinib and trastuzumab emtansine for patients with previously treated HER2-positive locally advanced and metastatic breast cancer: primary analysis of the randomized phase III trial HER2CLIMB-02. *Ann. Oncol.* **37** (3), 341–352. 10.1016/j.annonc.2025.11.005 (2026).
28. Liu, J. et al. Elucidating molecular mechanisms and therapeutic synergy: irreversible HER2-TKI plus T-Dxd for enhanced anti-HER2 treatment of gastric cancer. *Gastric Cancer*. **27** (3), 495–505. 10.1007/s10120-024-01478-6 (2024).
29. Mai, N. et al. ERBB2 Activating Mutations Promote Enhanced Internalization and Activity of Trastuzumab Deruxtecan in HER2-non-amplified Metastatic Breast Cancer. Clin Cancer Res (Epub ahead of print). (2026). 10.1158/1078-0432.CCR-26-0198
30. Modi, S. et al. Tucatinib in Combination With Trastuzumab Deruxtecan in Patients With Previously Treated HER2 + Unresectable Locally Advanced or Metastatic Breast Cancer: An Open-Label Phase 2 Study. *Clin. Breast Cancer*. **26** (8), 21–30. 10.1016/j.clbc.2026.05.010 (2026).
31. Mileva, M. et al. Molecular imaging predicts lack of T-DM1 response in advanced HER2-positive breast cancer (final results of ZEPHIR trial). *NPJ Breast Cancer*. **10** (1), 4. 10.1038/s41523-023-00610-6 (2024).
32. Rediti, M. et al. Integrating Molecular Imaging and Transcriptomic Profiling in Advanced HER2-Positive Breast Cancer Receiving Trastuzumab Emtansine: An Analysis of the ZEPHIR Clinical Trial. *Clin. Cancer Res.* **31** (1), 110–121. 10.1158/1078-0432.CCR-24-1007 (2025).
33. Girish, S. et al. Clinical pharmacology of trastuzumab emtansine (T-DM1): an antibody-drug conjugate in development for the treatment of HER2-positive cancer. *Cancer Chemother. Pharmacol.* **69** (5), 1229–1240. 10.1007/s00280-011-1817-3 (2012).
34. Lu, D. et al. Population pharmacokinetics of trastuzumab emtansine (T-DM1), a HER2-targeted antibody-drug conjugate, in patients with HER2-positive metastatic breast cancer: clinical

implications of the effect of covariates. *Cancer Chemother. Pharmacol.* **74** (2), 399–410. 10.1007/s00280-014-2500-2 (2014).

35. Li, C. et al. Exposure-response analyses of trastuzumab emtansine in patients with HER2-positive advanced breast cancer previously treated with trastuzumab and a taxane. *Cancer Chemother. Pharmacol.* **80** (6), 1079–1090. 10.1007/s00280-017-3440-4 (2017).
36. Chen, S. C. et al. Population pharmacokinetics and exposure-response of trastuzumab emtansine in advanced breast cancer previously treated with ≥ 2 HER2-targeted regimens. *Br. J. Clin. Pharmacol.* **83** (12), 2767–2777. 10.1111/bcp.13381 (2017).

Figures

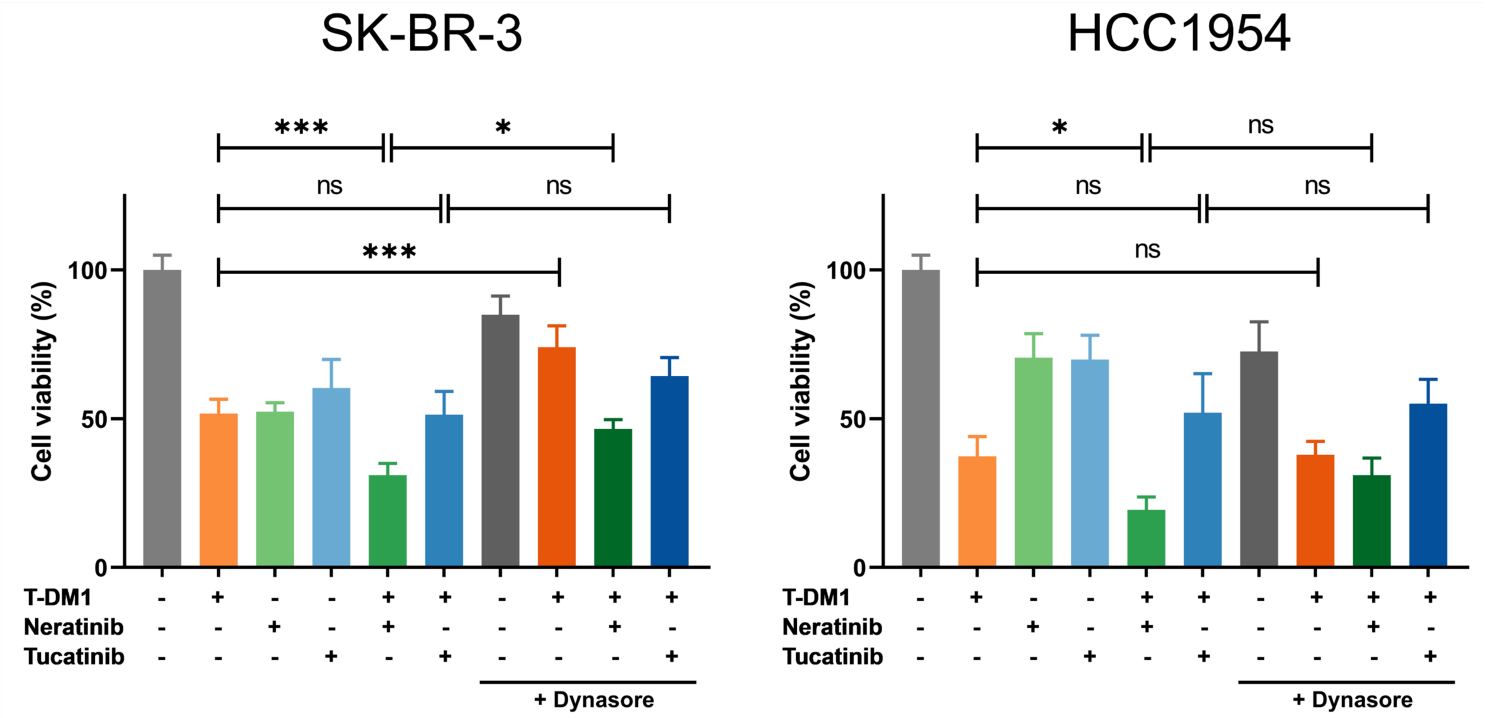


Figure 1

Effects of T-DM1 and HER2 kinase inhibitors on cell viability with or without dynasore. SK-BR-3 and HCC1954 cells were treated for 48 h with T-DM1 (0.04 µg/mL), neratinib (25 nM), tucatinib (300 nM), and the indicated combinations. Dynasore was used at 50 µM and 15 µM, respectively. Cell viability was determined using the Cell Counting Kit-8 assay and normalized to vehicle controls. Data are mean ± SD. *P < 0.05; **P < 0.01; ***P < 0.001; ns, not significant.

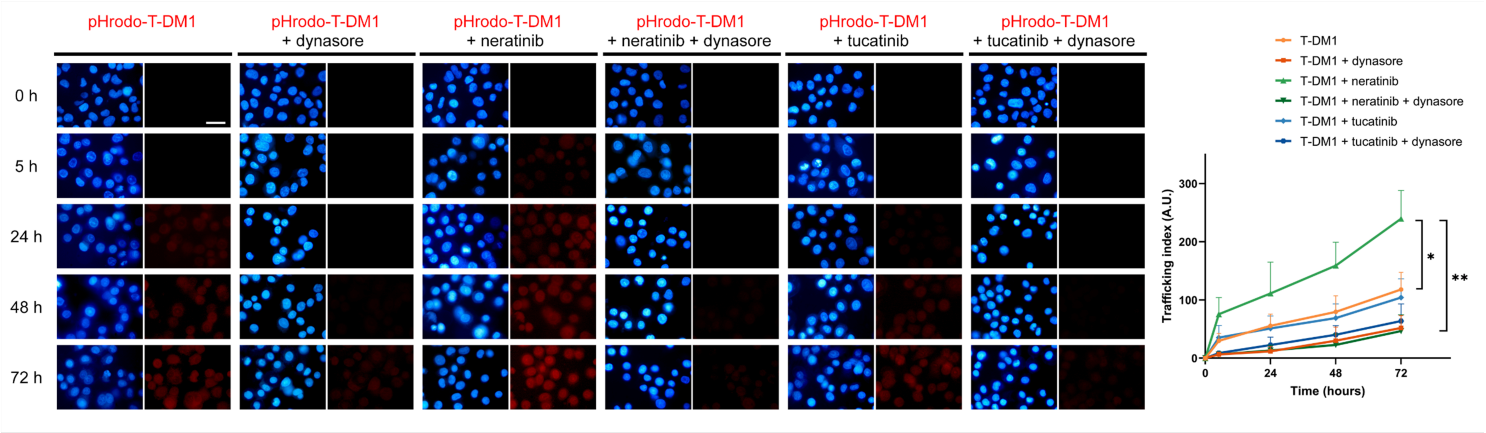


Figure 2

Acidification-associated trafficking of pHrodo-labeled T-DM1 in SK-BR-3 cells. Representative images show pHrodo-T-DM1 (0.05 μg/mL; red) with neratinib (25 nM), tucatinib (300 nM), and/or dynasore (50 μM) at 0, 5, 24, 48, and 72 h. Hoechst 33342 identifies nuclei (blue). Scale bar, 30 μm. The trafficking index is total cytoplasmic red fluorescence normalized to cell count. Data are mean ± SD. A.U., arbitrary units. *P < 0.05; **P < 0.01.

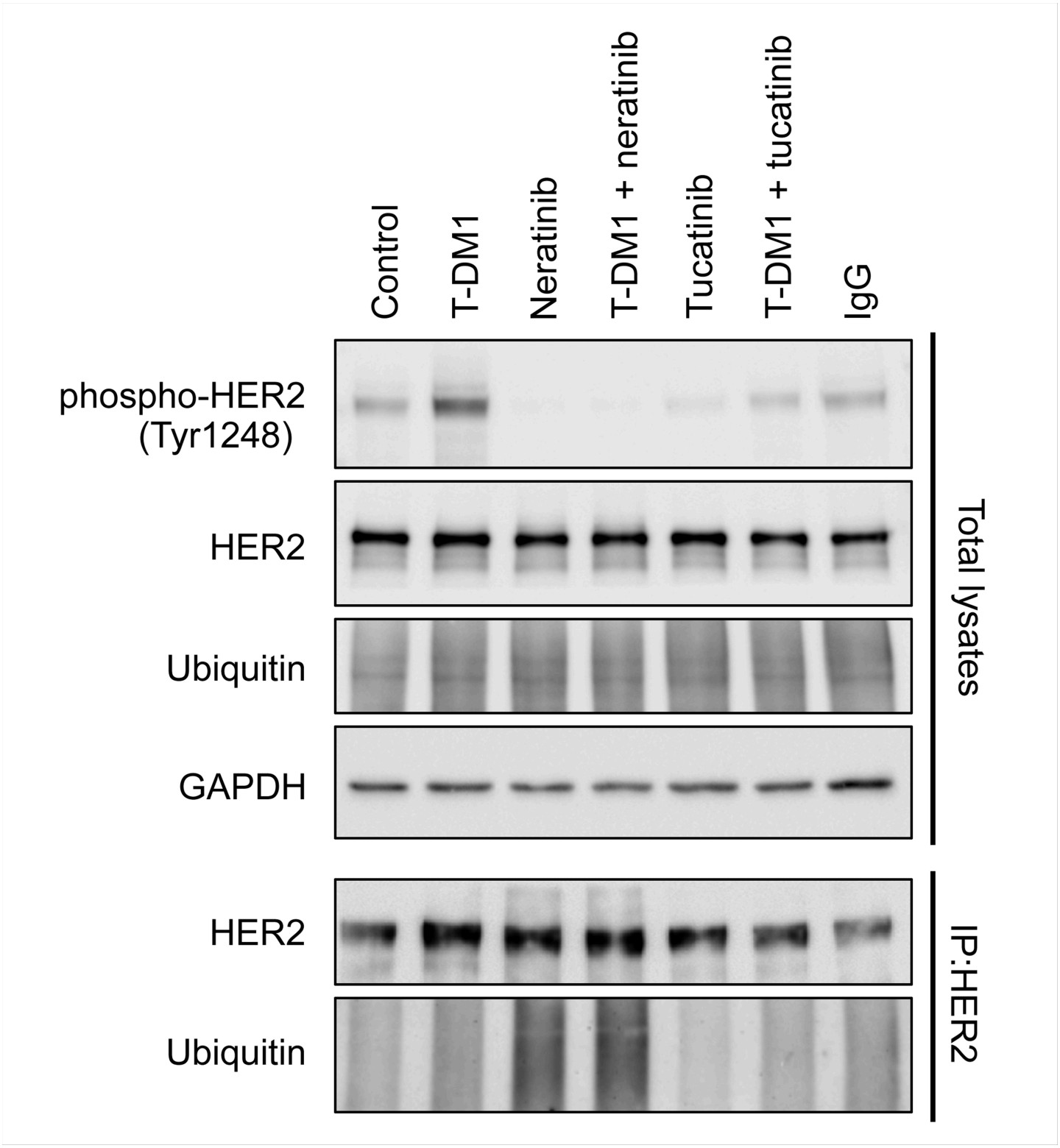


Figure 3

HER2 phosphorylation and HER2-associated ubiquitin after kinase-inhibitor treatment. SK-BR-3 cells were treated for 5 h with T-DM1 (0.05 μg/mL), neratinib (25 nM), tucatinib (300 nM), or their combinations. Whole-cell lysates were probed for phospho-HER2 Tyr1248, HER2, ubiquitin, and GAPDH. HER2 immunoprecipitates were probed for HER2 and ubiquitin. Normal IgG served as the

immunoprecipitation control. GAPDH is the whole-cell lysate loading control. Blots are representative of three independent experiments. IP, immunoprecipitation.

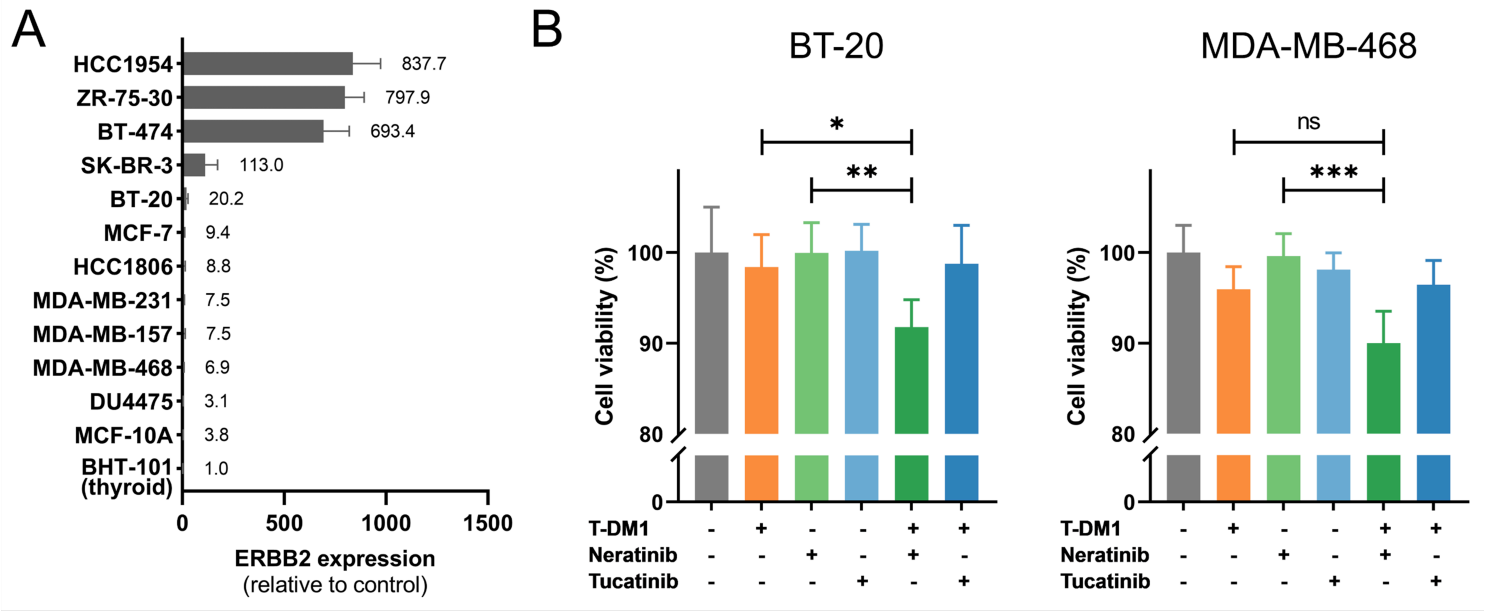


Figure 4

ERBB2 transcript expression and treatment responses in cells with lower ERBB2 expression. (A)Relative ERBB2 expression in the indicated cell lines measured by quantitative reverse transcription PCR, normalized to GAPDH and expressed relative to BHT-101, a thyroid cancer line. (B) Viability of BT-20 and MDA-MB-468 cells after 48 h of the indicated treatments, normalized to vehicle controls. Data are mean ± SD. *P < 0.05; **P < 0.01; ***P < 0.001; ns, not significant.

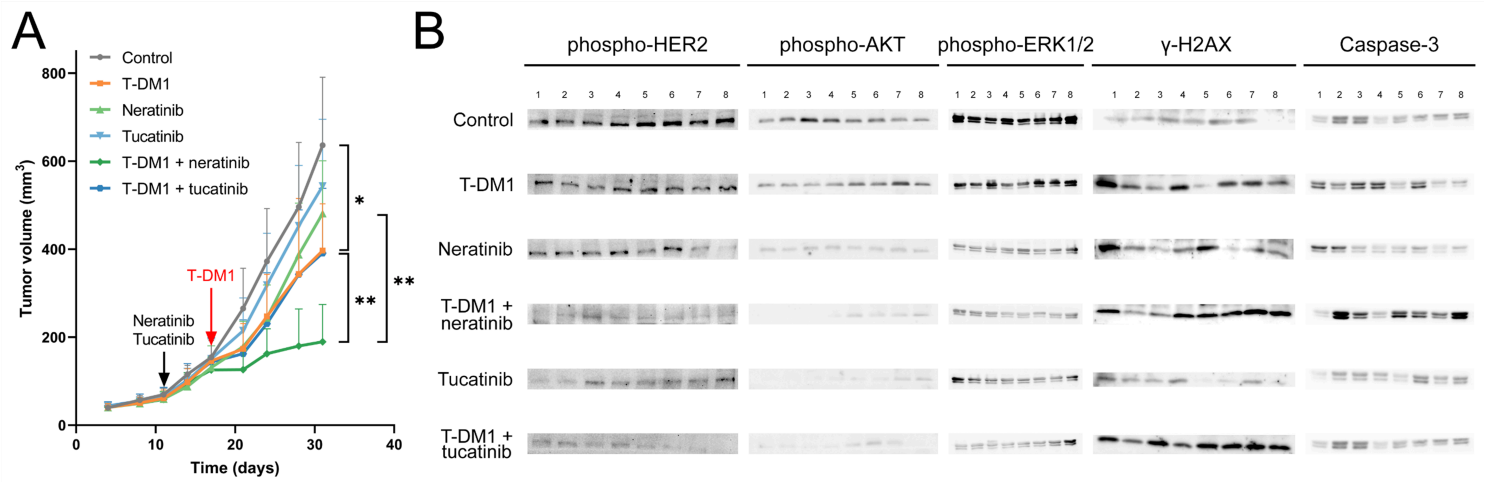


Figure 5

Antitumor activity in orthotopic HCC1954 xenografts. (A) Tumor volume in six treatment groups, with four mice per group bearing bilateral tumors. T-DM1 was administered at 0.5 mg/kg intravenously every 3 weeks; neratinib and tucatinib were each administered at 10 mg/kg orally five times per week. Arrows

indicate treatment initiation. Data are mean ± SD, calculated across four mice per group after averaging bilateral tumor volumes within each mouse at each time point. *P < 0.05; **P < 0.01. (B) Tumor immunoblots for phospho-HER2, phospho-AKT, phospho-ERK1/2, γ-H2AX, and cleaved caspase-3.

Supplementary Files

This is a list of supplementary files associated with this preprint. Click to download.

- Fullblots.pptx